Delft University of Technology

Analytical Formulas for Artificial Dielectrics with Nonaligned Layers

Cavallo, Daniele; Felita, Cantika

Important note
To cite this publication, please use the final published version (if applicable).
Please check the document version above.

Analytical Formulas for Artificial Dielectrics with Non-Aligned Layers

Daniele Cavallo, *Member, IEEE,* and Cantika Felita

Abstract— In this work, we present analytical models to describe artificial dielectric layers (ADLs), when a lateral shift between layers is present. The alternate lateral displacement between layers is an important parameter to engineer the desired effective electromagnetic properties of the equivalent homogeneous material realized with the ADLs. More specifically, the equivalent dielectric constants that can be realized by alternatively shifting the layers are higher compared to the aligned case. Closed-form expressions are derived for the equivalent layer reactance that includes the higher-order interaction between shifted layers. The given analytical formulas can be used to derive an equivalent circuit model that describes the scattering parameters of a plane wave impinging on a slab composed by an arbitrary finite number of metal layers. To aid the design of artificial dielectric slabs, the effective permittivity and permeability tensors are also retrieved from the scattering parameters.

Index Terms— Artificial dielectric, equivalent circuit, scattering from grids.

I. INTRODUCTION

ARTIFICIAL dielectrics (ADs) were introduced in [1] as a low-weight replacement to real dielectric materials, for realizing microwave lenses [2]. After their introduction, ADs have been extensively studied and used for decades in radar applications. An AD consists of a large-scale model of an actual dielectric, obtained by embedding conducting structures in a host material according to a regular pattern. The electric field scattered by the metallic inclusions, when added to the incident field, creates an effective equivalent delay [3]. At the frequencies for which the periodicity of the pattern is much smaller than the wavelength, the structure can be assigned equivalent parameters that describe a homogeneous dielectric. The effective electric parameters can be engineered by varying the size of the metal obstacles and their spatial density.

This work relates to a specific type of anisotropic ADs, which are realized as a cascade of planar layers made of sub-wavelength metal patches, as depicted in Fig. 1. Such structures are also referred to as artificial dielectric layers (ADLs).

Recently, ADLs have been employed as superstrates to improve the radiation performance of planar antennas, both in the microwave [4], [5] and the terahertz [6] frequency range.
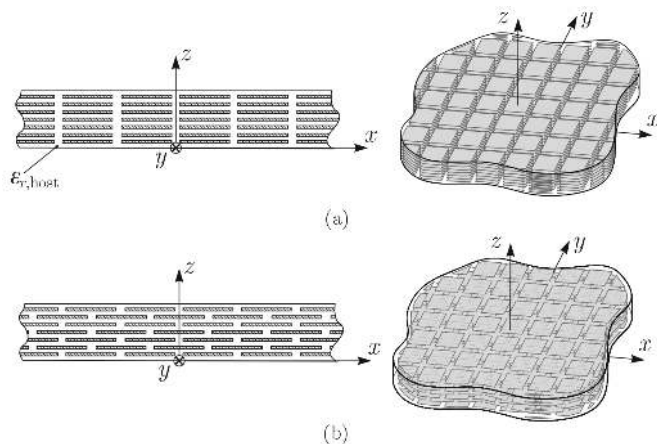
Fig. 1. Two-dimensional side view and three-dimensional prospective view for artificial dielectric slabs with (a) aligned layers and (b) with layers alternatively shifted in both x and y to increase the effective relative permittivity.

In these works, ADLs were exploited to enhance the front-to-back ratio of integrated antennas without supporting surface waves, with a consequent increase of gain and efficiency.

Several efficient numerical approaches can be employed to describe the scattering from ADL slabs [7]–[12]. These methods account for the higher-order interaction between layers, which cannot be neglected due to the electrically small inter-layer distance. A simplified analysis based on closed-form expressions was introduced in [13], [14], valid for the specific geometry in Fig. 1 in the low-frequency regime (sub-wavelength patches). However, while [14] only contemplates the case of aligned layers (arranged as in Fig. 1(a)), in this work we generalize the analysis to include the effects of alternate shifts, as shown in Fig. 1(b). This new configuration is very relevant for the design of ADLs, because the shift significantly increases the effective permittivity of the slab with respect to the aligned case.

The reason for the enhancement of the permittivity can be qualitatively explained by sketching the electric field distribution within two ADL structures, with and without shift, under normal plane-wave illumination. When a plane wave is impinging on the ADL structure, the electric field within the periodic unit cell can be represented with the vector field lines in Fig 2. In the aligned case, the field is mainly concentrated in the gaps between adjacent coplanar patches (Fig. 2(a)). On the contrary, the field in the shifted case is also distributed within the areas between parallel subsequent layers (Fig. 2(b)). Such behavior introduces an additional capacitance compared to the aligned setup, resulting in a higher equivalent permittivity.

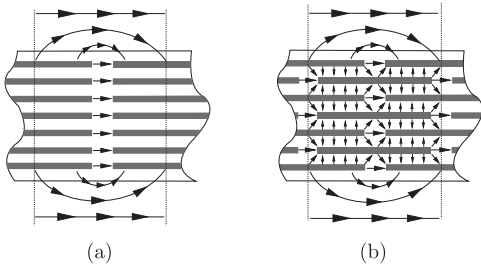Besides this qualitative explanation, a rigorous analysis is

Fig. 2. Electric field distribution for a plane wave propagating through the ADL slab for (a) aligned and (b) misaligned layers. In the first case, the electric field is mainly concentrated in the gaps between coplanar patches. In the second case the field is also strong in the vertical gaps between subsequent layers, resulting in a higher capacitive loading.

presented here, that provides closed-form expressions for the equivalent reactance of the layers, also valid for non-aligned cases. The reactances are then included in a simple analytical transmission-line model that describes the propagation, reflection and transmission of a plane wave impinging on an artificial dielectric slabs, for generic oblique incidence. This information can be used to derive the permittivity and permeability tensors of the artificial dielectric slabs using the method described in [15]. The variation of the effective constitutive tensors as a function of the different geometrical parameters of the ADLs is highlighted.

The main advantage of the formulation derived in this paper is the improved design flexibility. In fact, to tailor the equivalent dielectric constant in ADL slabs with aligned layers, one can vary geometrical parameters such as the inter-layer distance and the gap width between patches. However, these parameters cannot be freely changed, as they are typically limited by the technological constraints of the manufacturing process. On the contrary, the shift between layers represents an additional important degree of freedom that can be used for the design, as it greatly extends the ranges of permittivity values that can be synthesized, given a specific fabrication technology.

II. INTEGRAL EQUATION FOR SHIFTED ADLs

The analysis of ADLs with aligned layers was presented in [14]. In this section, we generalize the formulation to account for the shift between layers, omitting some of the steps of the method that are similar to [14].

A. Problem Definition and Equivalence Principle

Let us consider an ADL medium composed by an infinite number of layers spaced along z by distance d_z and numbered with consecutive integer indexes n_z, as shown in Fig. 3(a). The odd layers ($n_z = [...-3,-1,1,3,...]$) are shifted with respect to the even layers ($n_z = [...,-2,0,2,...]$) by s_x and s_y along x and y, respectively, as depicted in Fig. 3(b). We assume that a plane wave is traveling in the negative z-direction within the ADL medium, with electric and magnetic field indicated by $\mathbf{e}_i(x,y,z)$ and $\mathbf{h}_i(x,y,z)$, respectively (Fig. 4). By applying the equivalence theorem, we can define three surfaces S_1, S_0 and S_{-1} as shown in Fig. 5(a), denoting
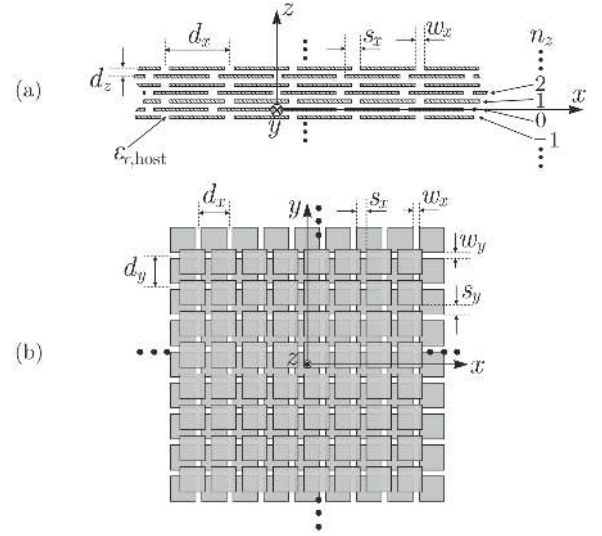

Fig. 3. Definition of the geometrical parameters characteristic of the shifted ADLs: (a) cross section and (b) top view.
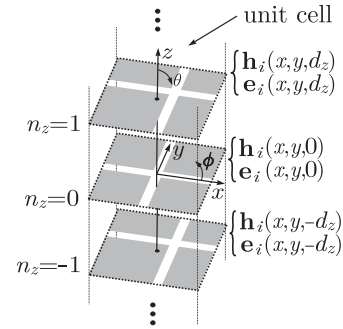
Fig. 4. Aperture fields on three layers of an infinite cascade of ADLs.
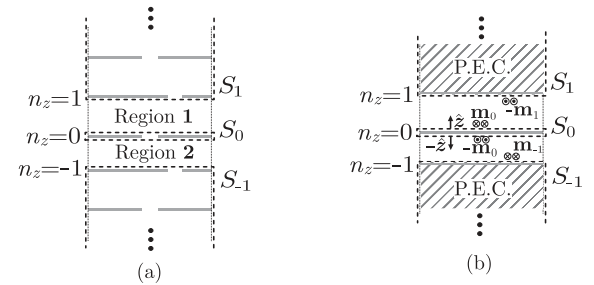
Fig. 5. (a) original problem and (b) equivalent problem with unknown magnetic current distributions.

with '1' and '2' the two regions above and below the layer located at $z = 0$. The volume bounded by the surfaces can be filled with a perfect electric conductor (P.E.C.), as shown in Fig. 5(b), according to the Schelkunoff's version of the equivalence principle [16], so that only equivalent surface magnetic currents $\mathbf{m}_{n_z}(x,y)$ are present in the regions corresponding with the gaps between patches in the initial problem. The equivalent magnetic currents are related to the aperture electric field as

$$\mathbf{m}(\boldsymbol{\rho},z=n_zd_z\pm\epsilon)=\mp\hat{\mathbf{z}}\times\mathbf{e}_i(\boldsymbol{\rho},z=n_zd_z\pm\epsilon)=\pm\mathbf{m}_{n_z}(\boldsymbol{\rho}) \quad (1)$$
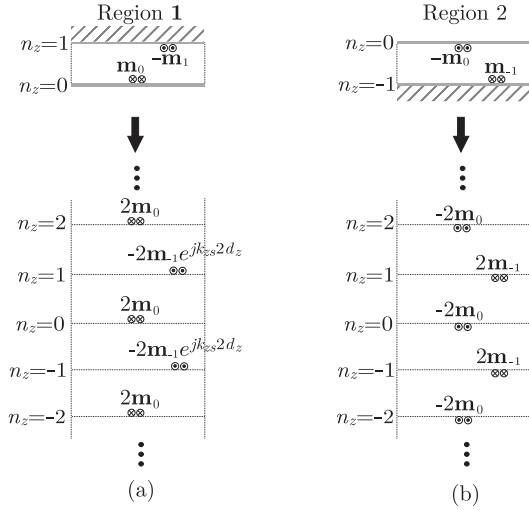
Fig. 6. Application of image theorem for (a) Region 1 and (b) Region 2, defined in Fig. 5.

Fig. 7. Normalized magnitude and phase of magnetic current distribution on the two orthogonal slot axes (red dashed line in the inset), comparing CST [17] with the approximation in (4): TE incidence along (a) x- and (b) y-slots, and TM incidence along (c) x- and (d) y-slots. The dimensions of the ADLs are $d_x = d_y = 0.0785\lambda_0$, $w_x = w_y = 0.0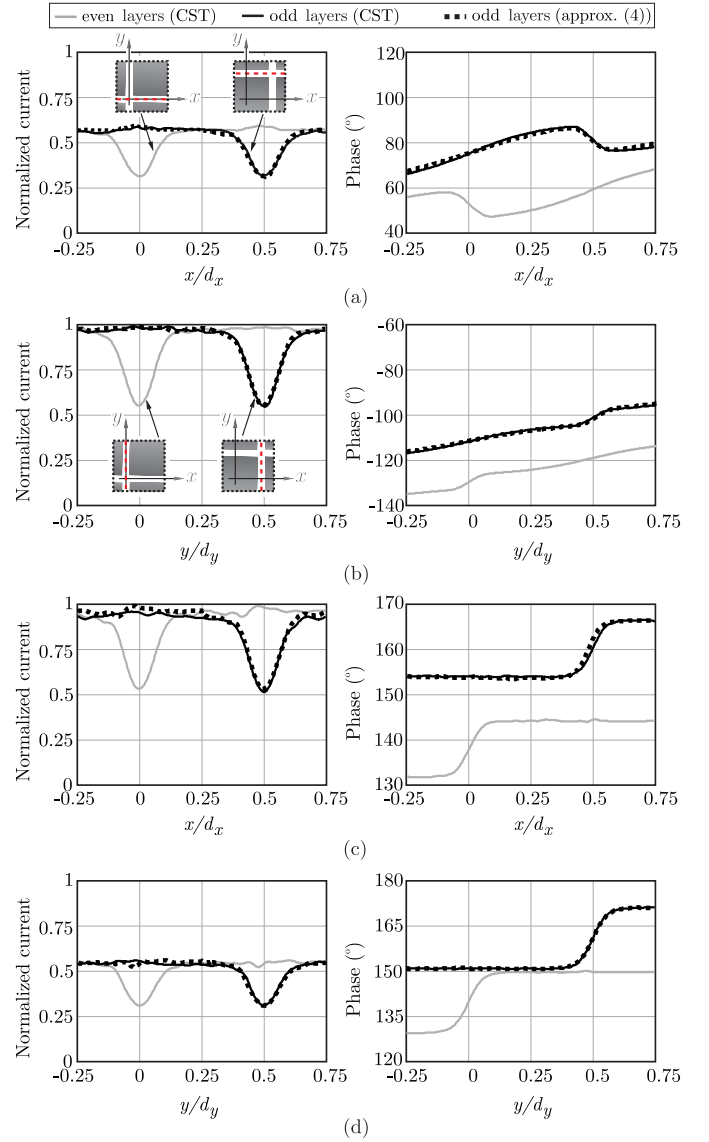1\lambda_0$, $d_z = 0.012\lambda_0$, $s_x = s_y = 0.5d_x$, with λ_0 being the wavelength at the calculation frequency. All figures refer to plane-wave incidence at $\theta = 60°$ and $\phi = 60°$.

where $\boldsymbol{\rho} = x\hat{\mathbf{x}} + y\hat{\mathbf{y}}$ and ϵ is a vanishingly small distance. It is evident from (1) that the two magnetic current distributions above and below the layer $n_z = 0$ are equal and opposite, since the normal unit vector changes sign and the tangential electric field is continuous in the gap.

Due to the periodicity along z, we can impose Floquet boundary conditions, i.e. the magnetic currents on the layers at $n_z = 1$ and $n_z = -1$ are related by a phase shift:

$$\mathbf{m}_1(\boldsymbol{\rho}) = \mathbf{m}_{-1}(\boldsymbol{\rho})e^{jk_{zs}2d_z} \qquad (2)$$

where k_{zs} is an unknown equivalent wavenumber describing the propagation along z. By applying the image theorem, we can replace the problem in Fig. 5(b) with an infinite sum of current contributions for the Region 1 and the Region 2, as depicted in Fig. 6. Hence, imposing the continuity of the transverse magnetic field at the layer at $z = 0$ leads to the following integral equation:

$$\sum_{n_z\text{even}} \int_{-\infty}^{\infty}\int_{-\infty}^{\infty} 4\mathbf{m}_0(\boldsymbol{\rho}')\mathbf{g}(\boldsymbol{\rho} - \boldsymbol{\rho}', n_z d_z, z=0)d\boldsymbol{\rho}' =$$

$$\sum_{n_z\text{odd}} \int_{-\infty}^{\infty}\int_{-\infty}^{\infty} 2(e^{jk_{zs}2d_z} + 1)\mathbf{m}_{-1}(\boldsymbol{\rho}')\mathbf{g}(\boldsymbol{\rho} - \boldsymbol{\rho}', n_z d_z, z=0)d\boldsymbol{\rho}'$$

$$(3)$$

where $\boldsymbol{\rho} = x\hat{\mathbf{x}} + y\hat{\mathbf{y}}$ and $\boldsymbol{\rho}' = x'\hat{\mathbf{x}} + y'\hat{\mathbf{y}}$ are the observation and the source points, respectively. The function $\mathbf{g}$ represents the free-space dyadic Green's function, which relates the magnetic field to a magnetic source.

B. Approximation on the Magnetic Current Distribution

Unlike the case of aligned layers in [14], the periodic cell is now a combination of two layers rather than one, thus we cannot relate the magnetic current $\mathbf{m}_0$ to $\mathbf{m}_{-1}$ using Floquet boundary conditions. However, to simplify the formulation and enable a closed-form solution for the equivalent layer reactance, we assume that the magnetic currents on the two layers are approximately equal in amplitude and differ only from a spatial displacement and a phase term:

$$\mathbf{m}_{-1}(\boldsymbol{\rho}') \approx \mathbf{m}_0(\boldsymbol{\rho}' - \mathbf{s})e^{-j\mathbf{k}_{\rho s}\cdot\mathbf{s}}e^{-jk_{zs}d_z} \qquad (4)$$

where $\mathbf{s} = s_x\hat{\mathbf{x}} + s_y\hat{\mathbf{y}}$ is the vector indicating the shift and $\mathbf{k}_{\rho s} = k_{xs}\hat{\mathbf{x}} + k_{ys}\hat{\mathbf{y}}$ is an unknown wave vector describing the transverse propagation between adjacent layers.

The approximation in (4) implies that the the field propagation from one layer to the next is dominated by a lossless guided phenomenon. To assess the error given by this assumption, Fig. 7 shows the normalized magnitude and the phase of the magnetic current on the two orthogonal slots (gaps between patches) on different layers. The magnetic current is observed

Fig. 9. Vector magnetic current density and electric field magnitude in correspondence of the junction, obtained with CST. The electric-field magnitude (proportional to the magnetic current) drops in the junction due to the widening of the magnetic current.
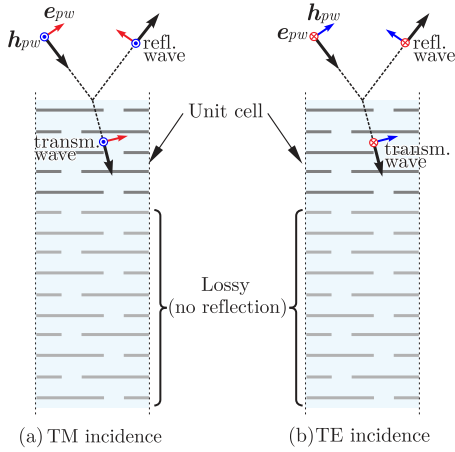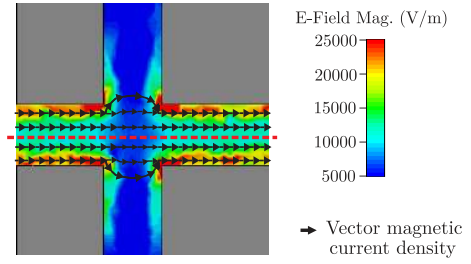
Fig. 8. Description of the CST models used to simulate a semi-infinite cascade of layers. A lossy ADL with the same geometrical parameters is implemented so that the transmitted wave experiences low reflection.

on the slots' axes, indicated by the dashed red lines in the inset of Figs. 7(a) and 7(b). The geometrical parameters are set as $d_x = d_y = 0.0785\lambda_0$, $w_x = w_y = 0.01\lambda_0$, $d_z = 0.012\lambda_0$, $s_x = s_y = 0.5d_x$, with λ_0 being the wavelength at calculation frequency. Transverse electric (TE) and transverse magnetic (TM) plane-wave illuminations from $\theta = 60°$ and $\phi = 60°$ are considered. The results are obtained with CST [17], performing the simulations as described in Fig. 8: a semi-infinite cascade of layers is replicated by considering a lossy section of ADLs that implements a low-reflection boundary condition for the transmitted wave. For all considered cases in Fig. 7, the approximation (4) reproduces well the real current distribution on the odd layers. The value of k_{zs} to be used in (4) was derived from the simulated phase shift between the currents on two consecutive odd layers ($\Delta\phi$), which according to (2) is equal to $(2k_{zs}d_z)$. The propagation constants k_{xs} and k_{ys} in (4) are instead selected as the one of the incident plane wave in the ADL host medium, i.e. $k_0 \sin\theta\cos\phi$ and $k_0\sin\theta\sin\phi$, respectively.

The amplitude drops of the current that can be observed in Fig. 7 in correspondence of the junctions are due to the fact that we are plotting the current only on the slot axis, while the transverse distribution widens in the junction. This effect can be observed from the vector magnetic current and the magnitude of the electric field simulated with CST in Fig. 9.

Under the approximation in (4), and assuming that the distance d_z between layers is electrically small so that $e^{\pm jk_{zs}d_z} \approx 1 \pm jk_{zs}d_z$, the integral equation in (3) becomes, after a few algebraic steps

$$\sum_{n_z \text{even}} \int_{-\infty}^{\infty}\int_{-\infty}^{\infty} 4\mathbf{m}_0(\boldsymbol{\rho}')\mathbf{g}(\boldsymbol{\rho}-\boldsymbol{\rho}', n_zd_z, z=0)d\boldsymbol{\rho}' -$$

$$\sum_{n_z \text{odd}} \int_{-\infty}^{\infty}\int_{-\infty}^{\infty} 4\mathbf{m}_0(\boldsymbol{\rho}'-\mathbf{s})e^{-j\mathbf{k}_{\rho s}\cdot\mathbf{s}}\mathbf{g}(\boldsymbol{\rho}-\boldsymbol{\rho}', n_zd_z, z=0)d\boldsymbol{\rho}' \approx 0 .$$

$$(5)$$

III. SOLUTION OF THE INTEGRAL EQUATION AND EQUIVALENT CIRCUIT

The approximated integral equation in (5) is written only in terms of the unknown magnetic current distribution on the layer $n_z = 0$. This condition allows to solve the equation with a procedure similar to the one described in [13], [14].

A. Expansion of the Magnetic Current and Admittance Matrix

In the low-frequency regime, for which the ADL period is small compared to the wavelength, the current can be expanded with four entire-domain basis functions:

$$\mathbf{m}_0(\boldsymbol{\rho}) = \sum_{p=1}^{4} a_p\mathbf{f}_p(\boldsymbol{\rho}) \qquad (6)$$

where a_p are unknown coefficients, and the basis functions are defined as in [13]:

$$\mathbf{f}_1(\boldsymbol{\rho}) = e^{-jk_{x0}x}\Pi_{w_y}(y)\hat{\mathbf{x}}, \quad \mathbf{f}_3(\boldsymbol{\rho}) = b_{d,x}(x)\Pi_{w_y}(y)\hat{\mathbf{x}}$$
$$\mathbf{f}_2(\boldsymbol{\rho}) = e^{-jk_{y0}y}\Pi_{w_x}(x)\hat{\mathbf{y}}, \quad \mathbf{f}_4(\boldsymbol{\rho}) = b_{d,y}(y)\Pi_{w_x}(x)\hat{\mathbf{y}} . \quad (7)$$

The longitudinal part of the functions $\mathbf{f}_1$ and $\mathbf{f}_2$ describes the linear phase progression of the magnetic current, induced by the incident plane wave, with wavenumbers k_{x0} and k_{y0} along x and y, respectively. The functions $\mathbf{f}_3$ and $\mathbf{f}_4$ represent anti-symmetric profiles, defined in [13](Eq. (13)), that characterize the magnetic current distribution at the junction between orthogonal slots. The transverse distribution on the slots is assumed to be constant, hence defined by the function $\Pi_w(\xi) = 1/w$ for $\xi \in [-w/2, w/2]$ and 0 elsewhere.

An expansion similar to (7) was used in [13], where only three unknowns were considered by imposing $a_3 = a_4$ to satisfy the Kirchhoff's law at the junction. However, such condition can be assumed for a single layer, but it is not valid in general for a multi-layer cascade, since also z-components of the electric field (between adjacent layers) are supported by the structure.

By substituting (6) in (5) and by applying Galerkin projection, we can define an admittance matrix $\overline{\overline{\mathbf{Y}}}$ which satisfies the homogeneous system of equations

$$\overline{\overline{\mathbf{Y}}}\,\overline{\mathbf{a}} = \mathbf{0} \qquad (8)$$

where $\overline{\mathbf{a}} = (a_1, a_2, a_3, a_4)^{\text{T}}$ is the vector of unknown coefficients.

B. Equivalent Reactance of ADLs

For deriving an equivalent model that describes the scattering of a plane wave impinging on the ADL structure, it is convenient to evaluate the admittance in the spectral domain, as described in Appendix A.

For the sake of simplicity and for enabling analytical solutions, we assume that the geometrical parameters are the same along x and y ($s_x = s_y = s$, $d_x = d_y = d$, $w_x = w_y = w$). The latter assumption refers to geometries with azimuthal invariance (scattering of a plane wave is independent of ϕ), for which TE and TM modes are decoupled. More general geometries can be still analyzed with the formalism of this paper, but they result in more complex equivalent networks that couple TE and TM modes and do not lend themselves to simple closed-form representations.

Under the condition $s_x = s_y$, it can be demonstrated (Appendix B) that the system of linear equations (8) is reduced to the following simpler problem

$$\overline{\overline{Y}}_{\text{TETM}} \, \overline{a}_{\text{TETM}} = 0 \tag{9}$$

where

$$\overline{a}_{\text{TETM}} = (a_1 \cos\phi + a_2 \sin\phi, -a_1 \sin\phi + a_2 \cos\phi)^{\text{T}}. \tag{10}$$

The admittance matrix $\overline{\overline{Y}}_{\text{TETM}}$ is a 2×2 diagonal matrix that can be split in two terms, i.e. $\overline{\overline{Y}}_{\text{TETM}} = \overline{\overline{Y}}_{\text{TL}} + \overline{\overline{Y}}_{\text{ADL}}$, as shown in Appendix B, leading to the equivalent circuit representation depicted in Fig. 10. The first contribution represents the propagation of the plane wave (fundamental Floquet wave) and can be represented as equivalent transmission lines, with characteristic impedance $Z_{0\text{TE}} = \zeta_0 / \cos\theta$ and $Z_{0\text{TM}} = \zeta_0 \cos\theta$ for the TE and TM modes, respectively, where k_0, ζ_0 are the free-space wavenumber and impedance. The second term is the equivalent admittance of one layer embedded in the infinite ADL cascade and can be approximated as

$$\overline{\overline{Y}}_{\text{ADL}} \approx \begin{bmatrix} jB_\infty (1 - \frac{\sin^2\theta}{2}) & 0 \\ 0 & jB_\infty \end{bmatrix}. \tag{11}$$

The equivalent layer susceptance in the presence of the shift is given by:

$$B_\infty \approx \frac{jk_0 d}{\zeta_0 \pi} \sum_{m \neq 0} \frac{|\text{sinc}(\pi m \frac{w}{d})|^2}{|m|} \cdot$$
$$\left(-\cot(-j2\pi|m|\frac{d_z}{d}) + e^{j2\pi m \frac{s}{d}} \csc(-j2\pi|m|\frac{d_z}{d}) \right) \tag{12}$$

where m are the indexes of the Floquet modes. The analytical expression in (12) accounts for the higher-order coupling between layers and thus remains valid even for inter-layer distances much smaller than the wavelength. It can be noted that the formula remains valid also for the aligned case $s_x = s_y = 0$.

While (12) is derived for an infinite number of layer, also the semi-infinite case is relevant to describe the effect of truncation in a finite cascade of layers. The susceptance of the first layer in a semi-infinite cascade is given by
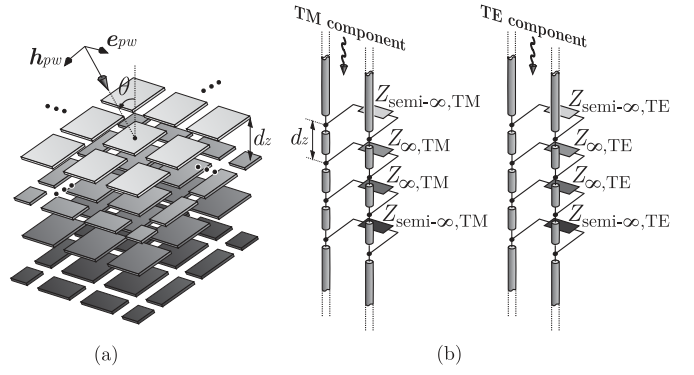

Fig. 10. (a) Plane wave impinging on a cascade of four ADLs with alternate shifts and (b) equivalent circuits for TE and TM components.

$$B_{\text{semi-}\infty} \approx \frac{jk_0 d}{2\zeta_0 \pi} \sum_{m \neq 0} \frac{|\text{sinc}(\pi m \frac{w}{d})|^2}{|m|} \cdot$$
$$\left(-j - \cot(-j2\pi|m|\frac{d_z}{d}) + e^{j2\pi m \frac{s}{d}} \csc(-j2\pi|m|\frac{d_z}{d}) \right). \tag{13}$$

C. Equivalent Transmission-Line Model

From eq. (11), one can express the reactance of a layer embedded in a periodic multi-layer environment as follows:

$$Z_{\infty,\text{TM}} = \frac{-j}{B_\infty}, \quad Z_{\infty,\text{TE}} = \frac{-j}{B_\infty(1 - \frac{\sin^2\theta}{2})}$$
$$Z_{\text{semi-}\infty,\text{TM}} = \frac{-j}{B_{\text{semi-}\infty}}, \quad Z_{\text{semi-}\infty,\text{TE}} = \frac{-j}{B_{\text{semi-}\infty}(1 - \frac{\sin^2\theta}{2})}. \tag{14}$$

These values of the equivalent reactance can be incorporated in an equivalent circuit that describes the propagation of a generic plane wave in the ADL medium. For example the cascade of four layers in Fig. 10(a) under plane-wave illumination can be represented as the equivalent transmission lines are shown in Fig. 10(b) for the TE and TM components. The infinite solution is used to represent the inner layers, whereas the semi-infinite formula is employed to characterize the edge layers, to account for the truncation.

To validate the formulas and assess the accuracy of the approximations, we show in Fig. 11 the reflection and transmission coefficients for TE and TM plane-wave incidence (at $\theta = 60°$) on a cascade of five layers, and for different values of the shifts. CST simulations are also reported for the same structures and show good agreement with our analytical transmission-line model.

D. Convergence Properties of the Floquet Sums

The sums in eqs. (12) and (13) contain an infinite number of terms. In practice, these sums are truncated to a finite number of Floquet modes $m \in [-M, -M+1, ..., -1, 1, 2, ..., M]$. To assess the convergence properties we define a relative difference between partial sums as follows:

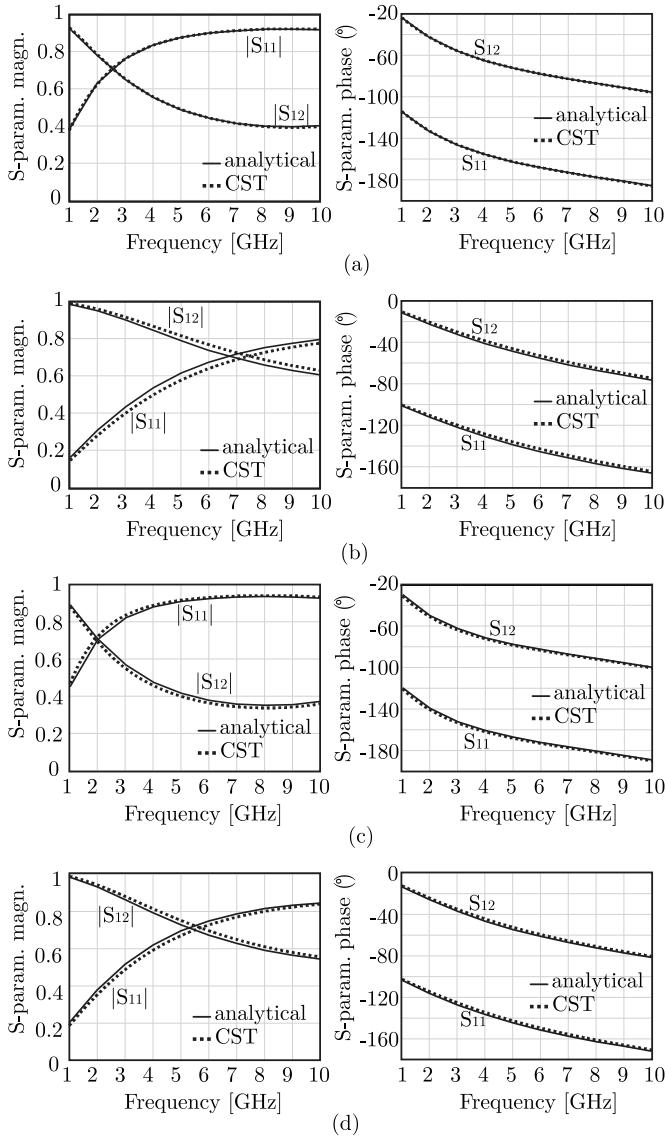$$\Delta = \frac{|B_\infty(M) - B_\infty(M-1)|}{|B_\infty(M)|} \tag{15}$$

Fig. 11. Amplitude and phase of the reflection and transmission coefficients of a plane wave incident on a cascade of 5 layers: (a) TE, $\theta = 60°$, $s = 0.25d$; (b) TM, $\theta = 60°$, $s = 0.25d$; (c) TE, $\theta = 60°$, $s = 0.5d$; (d) TM, $\theta = 60°$, $s = 0.5d$. The geometrical parameters are $d = 0.0785\lambda_0$, $w = 0.01\lambda_0$, $d_z = 0.012\lambda_0$, with λ_0 being the wavelength at 5 GHz.
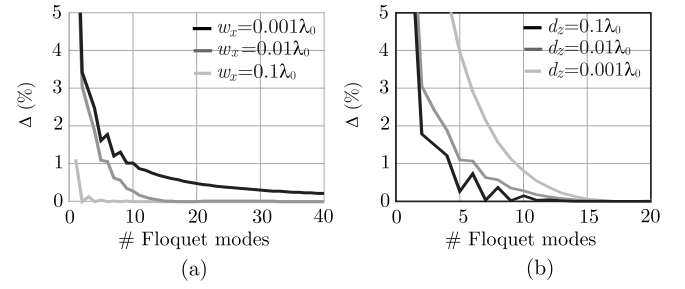

Fig. 12. Convergence characteristics, defined as in (15), of the susceptance B_∞ as a function of the number of Floquet modes: (a) $d_z = 0.01\lambda_0$ and three values of $w_x = w_y$ are considered; (b) $w_x, w_y = 0.01\lambda_0$ and three values of d_z are considered. The other parameters are $d_x = d_y = 0.2\lambda_0$ and $s_x = s_y = 0.45d_x$.
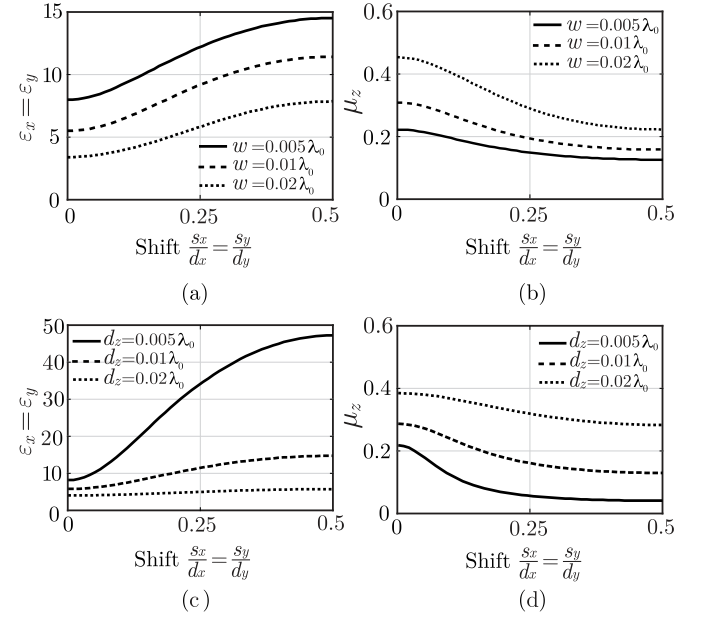

Fig. 13. Relevant components of the relative permittivity and permeability tensors, as a function of the shift: (a) and (b) refer to $d_z = 0.012\lambda_0$, with λ_0 being the wavelength at 5 GHz and three different values of w; (c) and (d) refer to $w = 0.01\lambda_0$ and three different values of d_z. For all figures, the ADL is composed of 5 layers embedded in a medium with $\varepsilon_{r,\text{host}} = 1$, with $d = 0.0785\lambda_0$.

where $B_\infty(M)$ represents the expression in (12) with the Floquet sum truncated from $-M$ to M modes. This convergence parameter of the susceptance B_∞ is shown in Fig. 12, for different geometrical parameters, as a function of the number of Floquet modes. It can be noted that the convergence is slower for small w_x, while smaller d_z lead actually to faster convergence. Despite the differences, all cases show rapid convergence for realistic design parameters, resulting in $\Delta < 1\%$ with only 10 modes or less.

IV. RETRIEVAL OF THE EFFECTIVE PARAMETERS

From the scattering parameters calculated using the equivalent circuit in Fig. 10(b), one can retrieve the effective permittivity and permeability, using the formalism introduced in [15]. Since the ADL is an anisotropic material, the equivalent medium is characterized by permittivity and permeability tensors

$$
\overline{\overline{\varepsilon}} = \varepsilon_0 \begin{pmatrix} \varepsilon_x & 0 & 0 \\ 0 & \varepsilon_y & 0 \\ 0 & 0 & \varepsilon_z \end{pmatrix}, \quad \overline{\overline{\mu}} = \mu_0 \begin{pmatrix} \mu_x & 0 & 0 \\ 0 & \mu_y & 0 \\ 0 & 0 & \mu_z \end{pmatrix}. \quad (16)
$$

The variation of the ε_x and μ_z as a function of the shift is reported in Fig. 13. The curves are shown for different values of the slot width (w) and for different values of the inter-layer distance (d_z). When $s_x = s_y$, because of the square symmetry of the structure, the condition $\varepsilon_x = \varepsilon_y$ is satisfied and the material is uniaxial. It is also evident that, for ADLs hosted in vacuum, we obtain $\varepsilon_z = 1$, because the z-component of the electric field does not interact with the horizontal patches. It can be noted that the permittivity components ε_x and ε_y increase with the shift, because of the raised mutual
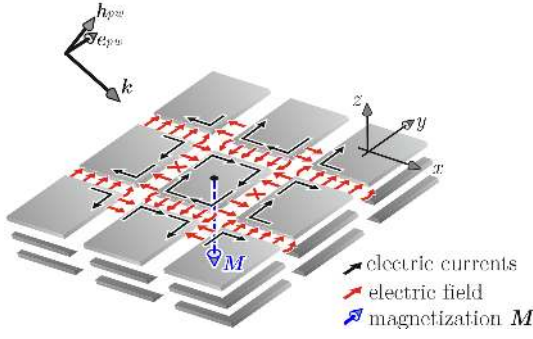
Fig. 14. Graphical interpretation of the diamagnetism of ADLs. In the case of TE incidence, the induced electric field distribution on a layer is compatible with loops of electric current on the metal patches, which in turn generate a magnetization field opposite to the magnetic field of the incident plane wave.

capacitance between layers. Moreover, smaller values of d_z lead to larger variation of permittivity as a function of the shift. Thus, for small inter-layer distances, very wide ranges of permittivity values can be synthesized by only varying the shift.

An opposite behavior is observed for the permeability component μ_z, which decreases as a function of the shift. Strong diamagnetic effects are occurring in the case of TE incidence, for which the incident magnetic field has a non-zero z-component. Indeed, in this case, the patches support loop currents that produce a magnetic field (magnetization) opposite to the incident one (see Fig. 14). Therefore, the total magnetic field inside the ADL is reduced compared to the external one (i.e., $\mu_z < 1$). The other components of the permeability tensors are $\mu_x = \mu_y = 1$.

Regarding the dispersion of ADLs, it can be pointed out that, under the assumption of sub-wavelength patches, the effective parameters are essentially constant with the frequency. Dispersive behavior occurs at higher frequencies, when the patches become comparable to the wavelength. However, the formulas derived in the paper are valid only under the assumption of sub-wavelength patches, which is valid in most practical ADL designs.

V. CONCLUSIONS

We derived closed-form formulas for the analysis of artificial dielectric layers (ADLs). The expressions of the equivalent reactance of each layer include the effect of an arbitrary diagonal shift between odd and even layers. The higher-order interaction between layers is rigorously accounted for in analytical form. The reactances can be embedded in an equivalent circuit that provides the scattering parameters for generic plane-wave incidence and for an arbitrary number of layers. The results given by our method were validated with simulations performed with commercial electromagnetic solvers. From the scattering parameters, the permittivity and permeability tensors can also be derived.

The presented analysis is functional to simpler and more flexible designs of ADLs, since the shift is a key parameter to achieve the desired effective constitutive properties.

APPENDIX A
SPECTRAL DOMAIN EXPRESSION OF THE ADMITTANCES

In this appendix we define the self and mutual admittances in the spectral domain, to allow for closed-form solution of the integral equation (5). The Fourier transforms of basis functions in (6) are given by

$$\mathbf{F}_1(k_{xm}, k_{ym}) = d_x \delta(m_x) \mathrm{sinc}(k_{ym} w_y/2) \hat{\mathbf{x}}$$
$$\mathbf{F}_2(k_{xm}, k_{ym}) = d_y \delta(m_y) \mathrm{sinc}(k_{xm} w_x/2) \hat{\mathbf{y}}$$
$$\mathbf{F}_3(k_{xm}, k_{ym}) = B_{d,x}(k_{xm}) \mathrm{sinc}(k_{ym} w_y/2) \hat{\mathbf{x}}$$
$$\mathbf{F}_4(k_{xm}, k_{ym}) = B_{d,y}(k_{ym}) \mathrm{sinc}(k_{xm} w_x/2) \hat{\mathbf{y}} \,. \quad (17)$$

where $k_{xm} = k_{x0} - 2\pi m_x/d_x$ and $k_{ym} = k_{y0} - 2\pi m_y/d_y$ are the Floquet wavenumbers with indexes m_x and m_y respectively, B_d is the Fourier transform of the doublet function and it is given by eq. (39) in [13], and δ is the Kronecker delta-function.

The terms of the admittance matrix are computed in the spectral domain as

$$Y_{qp} = -\frac{1}{d_x d_y} \sum_{m_x} \sum_{m_y} \mathbf{F}_q^*(-k_{xm}, -k_{ym}) \mathbf{G}(k_{xm}, k_{ym})\cdot$$
$$\mathbf{F}_p(k_{xm}, k_{ym}) S(k_{xm}, k_{ym}) \quad (18)$$

where 'p' and 'q' are the indexes of the basis and the test functions, respectively. Assuming that the ADLs are hosted in a homogeneous medium, in (18) we used the following property of the spectral dyadic Green's function $\mathbf{G}$:

$$\mathbf{G}(k_{xm}, k_{ym}, n_z d_z) = \mathbf{G}(k_{xm}, k_{ym}) e^{-jk_{zm}|n_z|d_z} \quad (19)$$

and we included all the sums on the n_z indexes in the following term:

$$S(k_{xm}, k_{ym}) = \sum_{n_z \text{even}} e^{-jk_{zm}|n_z|d_z} -$$
$$e^{j(k_{xm} - k_{xs})s_x} e^{j(k_{ym} - k_{ys})s_y} \sum_{n_z \text{odd}} e^{-jk_{zm}|n_z|d_z} \,. \quad (20)$$

From (39) and (40) in Appendix C, we can also express $S(k_{xm}, k_{ym})$ in closed form as

$$S(k_{xm}, k_{ym}) = -j \cot(k_{zm} d_z) +$$
$$j \csc(k_{zm} d_z) e^{j(k_{xm} - k_{xs})s_x} e^{j(k_{ym} - k_{ys})s_y} \,. \quad (21)$$

APPENDIX B
SIMPLIFIED ADMITTANCE MATRIX

The admittance matrix $\overline{\overline{\mathbf{Y}}}$ in (8) can be simplified by assuming, as in [13], that $B_{d,x}(k_{x0})$ and $B_{d,y}(k_{y0})$ are approximately 0. Such a condition applies because the projection of a progressive phase distribution (plane wave) onto an anti-symmetric function is negligible for electrically small periods. This assumption allows to neglect some terms of the admittance matrix $Y_{13} \approx Y_{31} \approx Y_{24} \approx Y_{42} \approx 0$. We also note that the self admittances Y_{44} and Y_{33} are equal, since the odd functions $\mathbf{f}_3$ and $\mathbf{f}_4$ are identical for $d_x = d_y$ and $w_x = w_y$.

With the previous hypotheses, we can then derive a reduced admittance matrix as

$$\overline{\overline{\mathbf{Y}}}_r = \begin{pmatrix} Y_{11} - \frac{Y_{41}Y_{14}Y_{33}}{Y_{33}^2 - Y_{34}Y_{43}} & Y_{12} + \frac{Y_{32}Y_{43}Y_{14}}{Y_{33}^2 - Y_{34}Y_{43}} \\ Y_{21} + \frac{Y_{41}Y_{23}Y_{34}}{Y_{33}^2 - Y_{34}Y_{43}} & Y_{22} - \frac{Y_{32}Y_{23}Y_{33}}{Y_{33}^2 - Y_{34}Y_{43}} \end{pmatrix} \quad (22)$$

which satisfies the relation

$$\overline{\overline{\mathbf{Y}}}_r \begin{pmatrix} a_1 \\ a_2 \end{pmatrix} = \mathbf{0}. \quad (23)$$

To investigate the ADL structure under TE and TM plane-wave incidence, it is convenient to project the equations on the TE and TM vectors. This can be done by introducing the rotation matrix

$$\mathbf{R} = \begin{pmatrix} \cos\phi & \sin\phi \\ -\sin\phi & \cos\phi \end{pmatrix}. \quad (24)$$

Pre-multiplying both the left and right hand sides of (23) by $\mathbf{R}$ and noting that $\mathbf{R}^{\mathrm{T}}\mathbf{R}$ is equal to the identity matrix $\mathbf{I}$, we can write

$$\mathbf{R}\,\overline{\overline{\mathbf{Y}}}_r\,\mathbf{R}^{\mathrm{T}}\,\mathbf{R}\begin{pmatrix} a_1 \\ a_2 \end{pmatrix} = \mathbf{0} \quad (25)$$

or

$$\overline{\overline{\mathbf{Y}}}_{\mathrm{TETM}}\begin{pmatrix} a_{\mathrm{TE}} \\ a_{\mathrm{TM}} \end{pmatrix} = \mathbf{0} \quad (26)$$

where we define $\overline{\overline{\mathbf{Y}}}_{\mathrm{TETM}} = \mathbf{R}\overline{\overline{\mathbf{Y}}}_r\mathbf{R}^{\mathrm{T}}$. The admittance matrix can be written as the sum of two contributions

$$\overline{\overline{\mathbf{Y}}}_{\mathrm{TETM}} = \overline{\overline{\mathbf{Y}}}_{\mathrm{TL}} + \overline{\overline{\mathbf{Y}}}_{\mathrm{ADL}}. \quad (27)$$

The first term is diagonal and represents the transmission lines describing the propagation of the plane wave:

$$\overline{\overline{\mathbf{Y}}}_{\mathrm{TL}} = \begin{bmatrix} \frac{2j\tan(k_{z0}\frac{d_z}{2})}{Z_{\mathrm{0TE}}} & 0 \\ 0 & \frac{2j\tan(k_{z0}\frac{d_z}{2})}{Z_{\mathrm{0TM}}} \end{bmatrix} \quad (28)$$

where $Z_{\mathrm{0TE}} = \zeta_0 k_0/k_{z0}$, $Z_{\mathrm{0TM}} = \zeta_0 k_{z0}/k_0$ are the characteristic impedances of the TE and TM transmission lines representing the plane-wave propagation; moreover, $k_{z0} = k_0\cos\theta$, and k_0, ζ_0 are the free-space wavenumber and impedance, respectively. For an infinite cascade of ADLs, $\overline{\overline{\mathbf{Y}}}_{\mathrm{TL}}$ represents two pairs of open stubs of length equal to half of the inter-layer spacing, as shown in Fig. 15. The second matrix in (28), $\overline{\overline{\mathbf{Y}}}_{\mathrm{ADL}}$, is the equivalent admittance of a single layer within the infinite cascade of ADLs. In the case of different shifts $s_x \neq s_y$, all the elements of this matrix are different from 0, thus the TE and TM component of the plane wave are coupled.

However, for $s_x = s_y$, it can be proved through a number of algebraic steps that the non-diagonal terms of $\overline{\overline{\mathbf{Y}}}_{\mathrm{ADL}}$ are approximately 0 and the matrix can be simplified as follows:

$$\overline{\overline{\mathbf{Y}}}_{\mathrm{ADL}} \approx \begin{bmatrix} jB_\infty(1 - \frac{\sin^2\theta}{2}) & 0 \\ 0 & jB_\infty \end{bmatrix} \quad (29)$$

where we define the slot susceptance as

$$B_\infty \approx \frac{jk_0 d_y}{\zeta_0 \pi} \sum_{m\neq 0} \frac{|\mathrm{sinc}(\pi m\frac{w_y}{d_y})|^2}{|m|} \cdot$$
$$\left(-\cot(-j2\pi|m|\frac{d_z}{d_y}) + e^{j2\pi m\frac{s_y}{d_y}}\csc(-j2\pi|m|\frac{d_z}{d_y})\right). \quad (30)$$
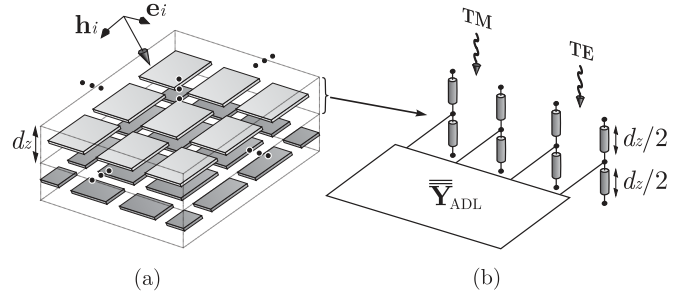

Fig. 15. Equivalent admittance of one layer of the ADLs embedded in an infinite cascade: (a) unit cell and (b) equivalent representation of the admittance matrix.

APPENDIX C
CLOSED FORM SOLUTIONS FOR INFINITE SUMS

The spectral domain integral equation contains a number of infinite sums over even and odd indexes, embedded in the function $S(k_{xm}, k_{ym})$ defined in (20). The purpose of this appendix is to derive closed form expression for these sums both for infinite or semi-infinite cascades of ADLs.

The semi-infinite sums over even indexes (from 0 to $+\infty$) and odd indexes (from 1 to $+\infty$) are given by

$$\sum_{n_z(\mathrm{even})=0}^{\infty} e^{-jk_{zm}|n_z|d_z} = 1 + e^{-jk_{zm}2d_z} + e^{-jk_{zm}4d_z} + \dots \quad (31)$$

$$\sum_{n_z(\mathrm{odd})=1}^{\infty} e^{-jk_{zm}|n_z|d_z} = e^{-jk_{zm}d_z} + e^{-jk_{zm}3d_z} + \dots. \quad (32)$$

With the change of variable $n_z' = n_z/2$, (31) can be expressed as

$$\sum_{n_z(\mathrm{even})=0}^{\infty} e^{-jk_{zm}|n_z|d_z} = 1 + \sum_{n_z'=1}^{\infty} e^{-jk_{zm}2|n_z'|d_z}. \quad (33)$$

By using the following known identities [3]:

$$\sum_{n=1}^{\infty} e^{jnx} = -\frac{1}{2} + \frac{j}{2}\cot\frac{x}{2}, \qquad \sum_{x(\mathrm{odd})=1}^{\infty} e^{jnx} = \frac{j}{2}\csc x \quad (34)$$

(33) and (32) can be evaluated as

$$\sum_{n_z(\mathrm{even})=0}^{\infty} e^{-jk_{zm}|n_z|d_z} = \frac{1}{2} - \frac{j}{2}\cot(k_{zm}d_z) \quad (35)$$

$$\sum_{n_z(\mathrm{odd})=1}^{\infty} e^{-jk_{zm}|n_z|d_z} = -\frac{j}{2}\csc(k_{zm}d_z) \quad (36)$$

The solution for the infinite sums can be derived from the semi-infinite ones by noting that

$$\sum_{n_z,\mathrm{even}} e^{-jk_{zm}|n_z|d_z} = 2\sum_{n_z(\mathrm{even})=0}^{\infty} e^{-jk_{zm}|n_z|d_z} - 1 \quad (37)$$

$$\sum_{n_z,\mathrm{odd}} e^{-jk_{zm}|n_z|d_z} = 2\sum_{n_z(\mathrm{odd})=1}^{\infty} e^{-jk_{zm}|n_z|d_z}. \quad (38)$$

which leads to

$$\sum_{n_z,\text{even}} e^{-jk_{zm}|n_z|d_z} = -j\cot(k_{zm}d_z) \qquad (39)$$

$$\sum_{n_z,\text{odd}} e^{-jk_{zm}|n_z|d_z} = -j\csc(k_{zm}d_z). \qquad (40)$$

References

[1] W. E. Kock, "Metallic delay lenses," *Bell System Tech. J.*, vol. 27, no. 1, pp. 58-82, Jan. 1948.

[2] S. S. D. Jones and J. Brown, "Metallic delay lenses," *Nature*, vol. 163, no. 4139, pp. 324325, Feb. 1949.

[3] R. E. Collin, *Field Thery of Guided Waves, 2nd Ed.* IEEE Press, New York, 1990.

[4] W. H. Syed and A. Neto, "Front-to-back ratio enhancement of planar printed antennas by means of artificial dielectric layers," *IEEE Trans. Antennas Propag.*, vol. 61, no. 11, pp. 5408-5416, Nov. 2013.

[5] W. H. Syed, D. Cavallo, H. Thippur Shivamurthy, and A. Neto, "Wideband, wide-scan planar array of connected slots loaded with artificial dielectric superstrates," *IEEE Trans. Antennas Propag.*, vol. 64, no. 2, pp. 543-553, Feb. 2016.

[6] W. H. Syed, G. Fiorentino, D. Cavallo, M. Spirito, P. M. Sarro, and A. Neto, "Design, fabrication and measurement of 0.3 THz on-chip double-slot antenna enhanced by artificial dielectrics," *IEEE Trans. THz Sci. Tech.*, vol. 5, no. 2, pp. 288-298, Mar. 2015.

[7] S. Monni, G. Gerini, A. Neto, and A. G. Tijhuis, "Multimode Equivalent Networks for the Design and Analysis of Frequency Selective Surfaces," *IEEE Trans. Antennas Propag.*, vol. 55, no. 10, pp. 2824-2835, Oct. 2007.

[8] F. Costa, A. Monorchio and G. Manara, "Efficient analysis of frequency-selective surfaces by a simple equivalent-circuit model," *IEEE Antennas Propag. Mag.*, vol. 54, no. 4, pp. 35-48, Aug. 2012.

[9] E. Martini, G. M. Sardi, and S. Maci, "Homogenization processes and retrieval of equivalent constitutive parameters for multisurface-metamaterials," *IEEE Trans. Antennas Propag.*, vol. 62, no. 4, pp. 2081-2092, Apr. 2014.

[10] R. Rodriguez-Berral, F. Mesa and F. Medina, "Analytical multimodal network approach for 2-D arrays of planar patches/apertures embedded in a layered medium," *IEEE Trans. Antennas Propag.*, vol. 63, no. 5, pp. 1969-1984, May 2015.

[11] R. Kuse, T. Hori, M Fujimoto, T. Seki, K. Sato, and I. Osima, "Equivalent circuit analysis of meta-surface using double-layered patch-type FSS," *IEICE Trans. Communications*, vol. 99B, no. 11, pp. 2373-2380, Nov. 2016.

[12] S. Barzegar-Parizi and B. Rejaei, "Calculation of effective parameters of high permittivity integrated artificial dielectrics," *IET Microw. Antennas Propag.*, vol. 9, no. 12, pp. 1287-1296, Sep. 2015.

[13] D. Cavallo, W. H. Syed, and A. Neto, "Closed-form analysis of artificial dielectric layers−Part I: Properties of a single layer under plane-wave incidence," *IEEE Trans. Antennas Propag.*, vol. 62, no. 12, pp. 6256-6264, Dec. 2014.

[14] D. Cavallo, W. H. Syed, and A. Neto, "Closed-form analysis of artificial dielectric layers−Part II: Extension to multiple layers and arbitrary illumination," *IEEE Trans. Antennas Propag.*, vol. 62, no. 12, pp. 6265-6273, Dec. 2014.

[15] D. Cohen and R. Shavit, "Bi-anisotropic metamaterials effective constitutive parameters extraction using oblique incidence S-parameters method," *IEEE Trans. Antennas Propag.*, vol. 63, no. 5, pp. 2071-2078, May 2015.

[16] S. A. Schelkunoff, "Some equivalence theorems of electromagnetics and their application to radiation problems," *Bell System Tech. J.*, vol. 15, pp. 92112, 1936.

[17] CST Microwave Studio, CST [Online]. Available: http://www.cst.com/

Daniele Cavallo (S'09−M'11) received the M.Sc. degree (*summa cum laude*) in telecommunication engineering from the University of Sannio, Benevento, Italy, in 2007, and his Ph.D. degree (*cum laude*) in electromagnetics from Eindhoven University of Technology (TU/e), Eindhoven, Netherlands, in 2011.

From January 2007 to November 2011, he was with the Antenna Group at the Netherlands Organization for Applied Scientific Research (TNO Defense, Security and Safety), The Hague, Netherlands. From 2012 to 2015, he was Postdoc at Delft University of Technology (TUDelft), Delft, Netherlands. In 2015, he visited Chalmers University of Technology in Gothenburg, Sweden. He is now assistant professor at TUDelft. He is the author or coauthor of about 100 papers published in peer-reviewed international journals and conference proceedings. His research interests include analytical and numerical methods for antenna characterization and the design of antenna arrays and on-chip antennas.

Dr. Cavallo was first author of the paper awarded with The Best Innovative Paper Prize at the 30th ESA Antenna Workshop in 2008 and received The Best Paper Award in Electromagnetics and Antenna Theory at the 11th European Conference on Antennas and Propagation (EuCAP) in 2017. The students he supervised received The Best Student Paper Award at EuCAP 2013, the "Special Mention" at EuCAP 2015 and the Else Kooi Prize in 2016. He has been awarded a 3-year personal grant from the Netherlands Organization for Scientific Research (NWO VENI, 250 keuro), for developing Efficient On-Chip Antennas for Terahertz Applications. He is currently an associate editor of the IEEE Transactions on Antennas and Propagation.

Cantika Felita received the B.Eng. degree (*cum laude*) in electrical engineering from the University of Indonesia, Depok, Indonesia, in 2013.

From 2013 to 2015, she joined Nokia in Jakarta, working on wireless telecommunications systems. She is currently pursuing her Master Degree at the Terahertz Sensing Group in TUDelft. Her research interests include the analysis and the characterization of artificial dielectrics.

She was co-recipient of The Best Paper Award in Electromagnetics and Antenna Theory at the 11th European Conference on Antennas and Propagation (EuCAP) in 2017.